Supporting Information

Metal-Organic Frameworks/Polythiophene Derivative: Neuron-Like S-Doped Carbon 3D Structure with Outstanding Sodium Storage Performance

Wen Zhong[a], Xingshuai Lv [b], Qianwu Chen[a], Manman Ren[a,d], Weiliang Liu[a], Guangda Li[a], Jiaoxian Yu[a], Mei Li [a], Ying Dai[b] *, Lianzhou Wang[c]**

[a] School of Materials Science and Engineering, Qilu University of Technology (Shandong Academy of Sciences), Jinan 250353, PR China

[b] School of Physics, State Key Laboratory of Crystal Materials, Shandong University, 250100 Jinan, PR China

[c] School of Chemical Engineering and Australian Institute for Bioengineering and Nanotechnology, The University of Queensland, QLD 4072, Australia

[d] Key Laboratory of Advanced Energy Materials Chemistry (Ministry of Education), College of Chemistry, Nankai University, Tianjin 300071, China

***Email:** renmanman@qlu.edu.cn

***Email:** daiy60@sdu.edu.cn

***Email:** l.wang@uq.edu.au

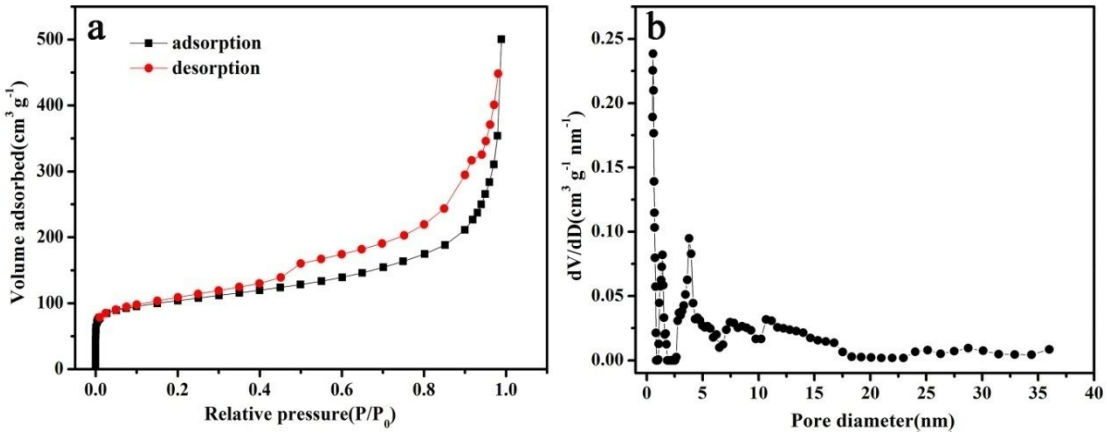

Figure S1. a) Nitrogen adsorption-desorption isotherm and b) the pore size distribution profile of MDC-700.

Nitrogen adsorption-desorption isotherm in Figure S1a indicates that the isotherm of MDC-700 is IV type. MDC-700 possesses a specific surface area of 377 m^2/g. Pore size distribution profile (Figure S1b) manifests that the presence of micropores and mesoporous in MDC-700 architecture.

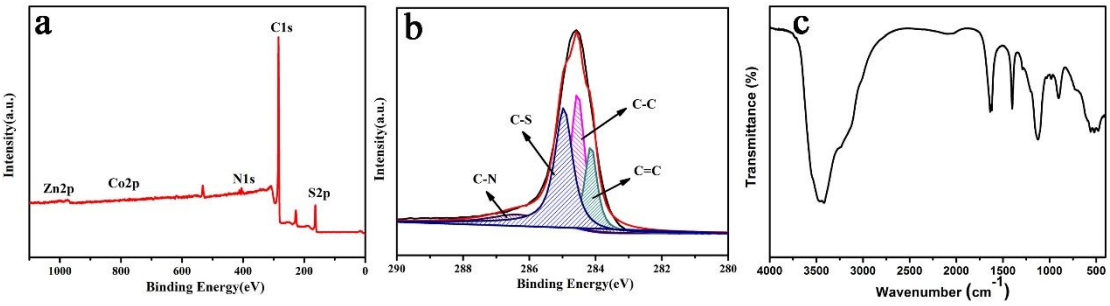

Figure S2. a) XPS wide spectrum, b) C1s XPS spectrum and c) FTIR spectra of the 3DSC-700.

As illustrated in Figure S2a, the wide spectrum manifests that the 3DSC-700 contains C, N, S, Co and Zn elements. There are four fitted peaks located at 286.4, 284.9, 284.5 and 284.1 eV in C1s spectrum (Figure S2b) which are ascribed to C-N groups, C-S, C-C, and C=C respectively.[1] Figure S2c shows the FTIR spectra of the 3DSC-700 electrode, the peak centered at 1119 cm^{-1} correspond to the stretching vibration band of

C-S-C.[2]

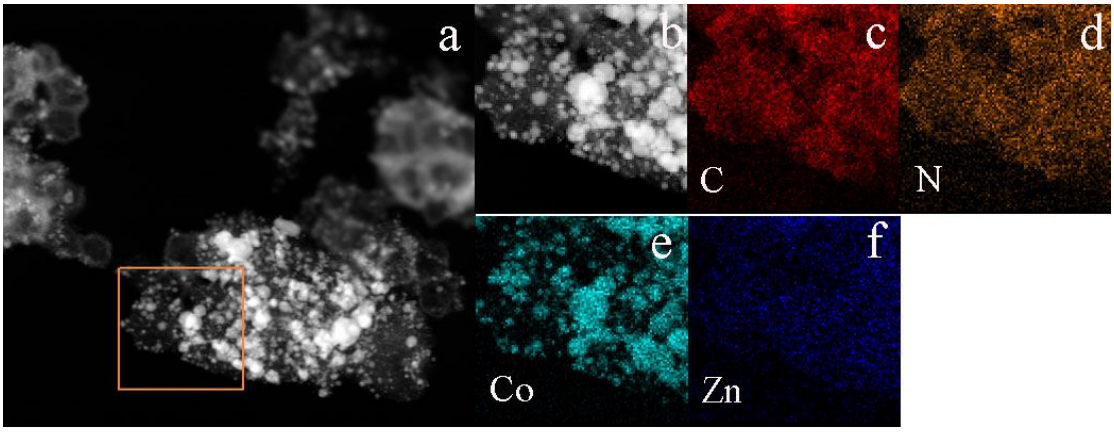

Figure S3. a) Drift-corrected image scanning and b) HAADF-STEM image of MDC-700. EDS elemental mapping images of c) carbon, d) nitrogen, e) cobalt, and f) zinc.

Figure S3a~f present the drift corrected spectrum image scanning, HAADF-STEM image and EDS element mapping of the MDC-700. EDS elemental mapping exhibit the uniformly distribution of c) carbon, d) nitrogen, e) cobalt and f) zinc. The N, Co and Zn come from the ZIF-8/ZIF-67 precursor.

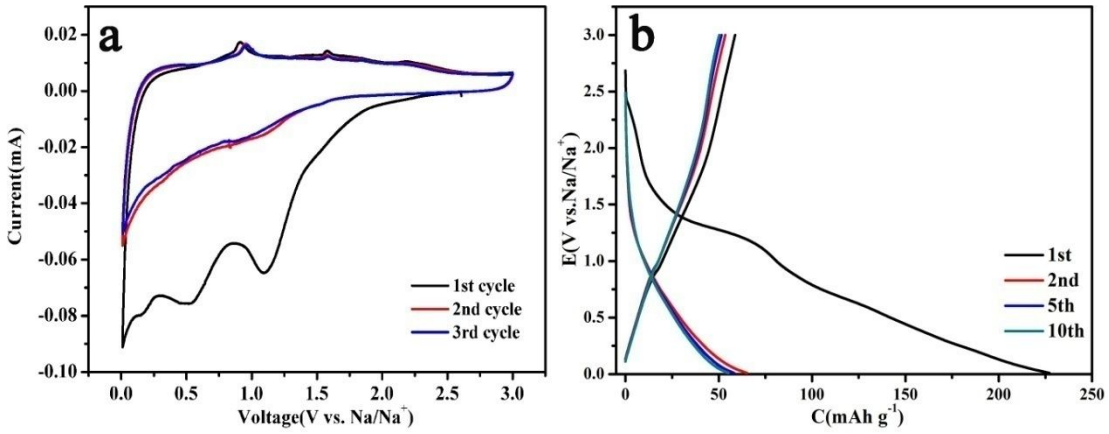

Figure S4. a) Cyclic voltammetry curves of MDC-700 in a potential range of 0.01-3.0 V (vs Na/Na^+) at a scan rate of 0.1 mV/s and b) discharge-charge curves of MDC-700 in a potential range of 0.01-3.0 V (vs Na/Na^+) at a current density of 100 mA/g.

For MDC-700 electrode, there are four peaks located at 1.2, 0.6, 0.28 and 0 V in the

first cathodic scan, which can be attributed to the irreversible reactions in the surface of MDC-700, the formation of solid electrolyte interface (SEI) and the insertion of sodium ions into MDC-700 interlayer, respectively (Figure S4a).[3-4] The anodic peak at 0.85 V in MDC-700 electrode is mostly related to the reversible reaction between Na^+ and N functional groups. The initial charge/discharge capacities of MDC-700 (Figure S4b) are 58.7/227.1 mAh/g.

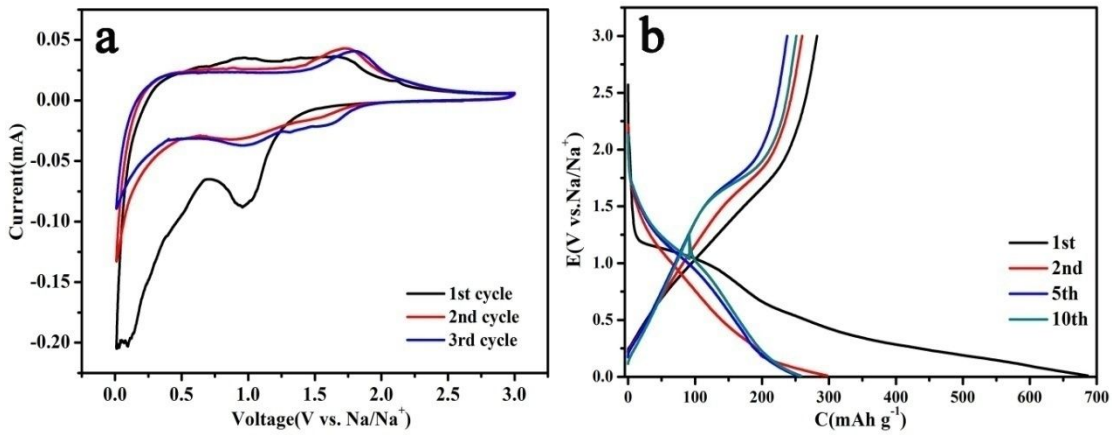

Figure S5. a) Cyclic voltammetry curves of SC-700 in a potential range of 0.01-3.0 V (vs Na/Na^+) at a scan rate of 0.1 mV/s and b) discharge-charge curves of SC-700 in a potential range of 0.01-3.0 V (vs Na/Na^+) at a current density of 100 mA/g.

As the Figure S5a shows, compared with MDC-700, the SC-700 electrode exhibits other two pairs of redox peaks centered at 1.75/2.15 V and 1.15/1.80 V, which is similar with room temperature Na-S batteries and can be ascribed to the Faradaic reactions between the Na^+ and covalent sulfur.[5-6] The initial charge/discharge capacities of SC-700 (Figure S5b) are 282.1/686.3 mAh/g, respectively.

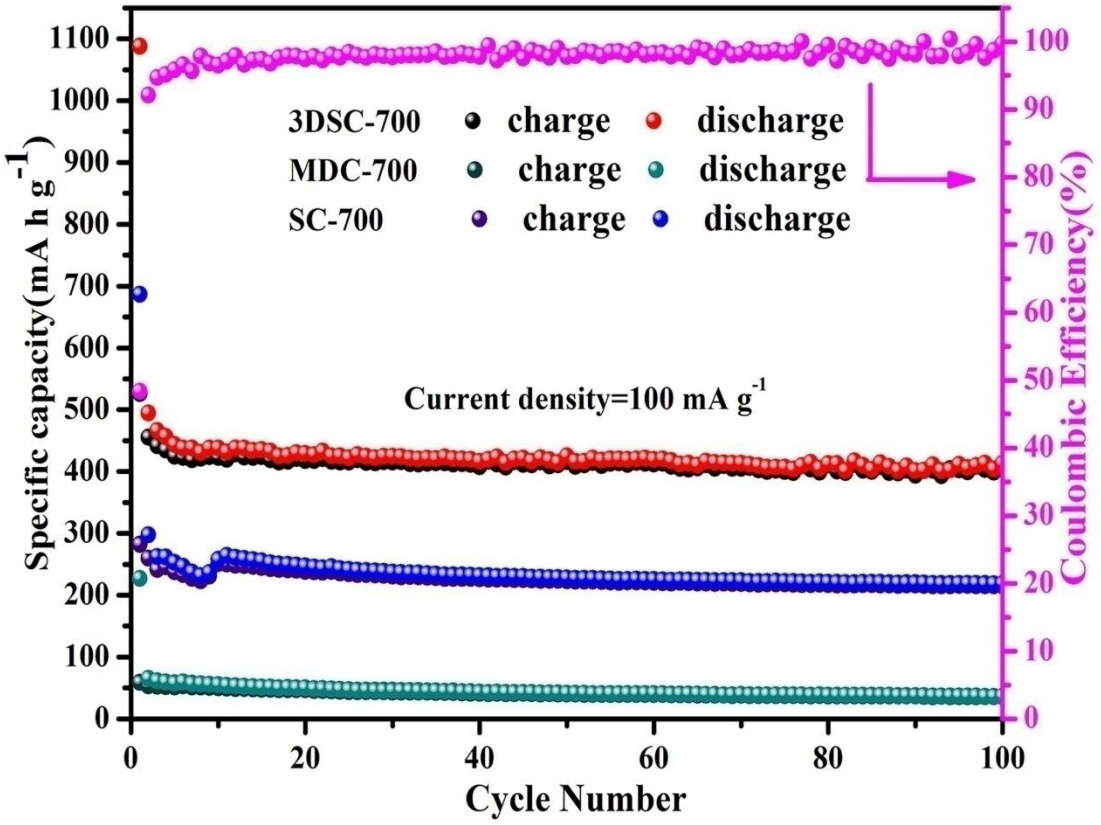

Figure S6. Cycling stability of 3DSC-700, MDC-700 and SC-700 at a current density of 100 mA/g.

As the Figure S6 shows, when tested at 100 mA/g, a high reversible capacity of ~ 450 mAh/g can be obtained for the 3DSC-700 after 100 cycles with almost 100 % Coulombic efficiency, while the capacities of MDC-700 and SC-700 after 100 cycles are 36.4 and 216.9 mAh/g, respectively.

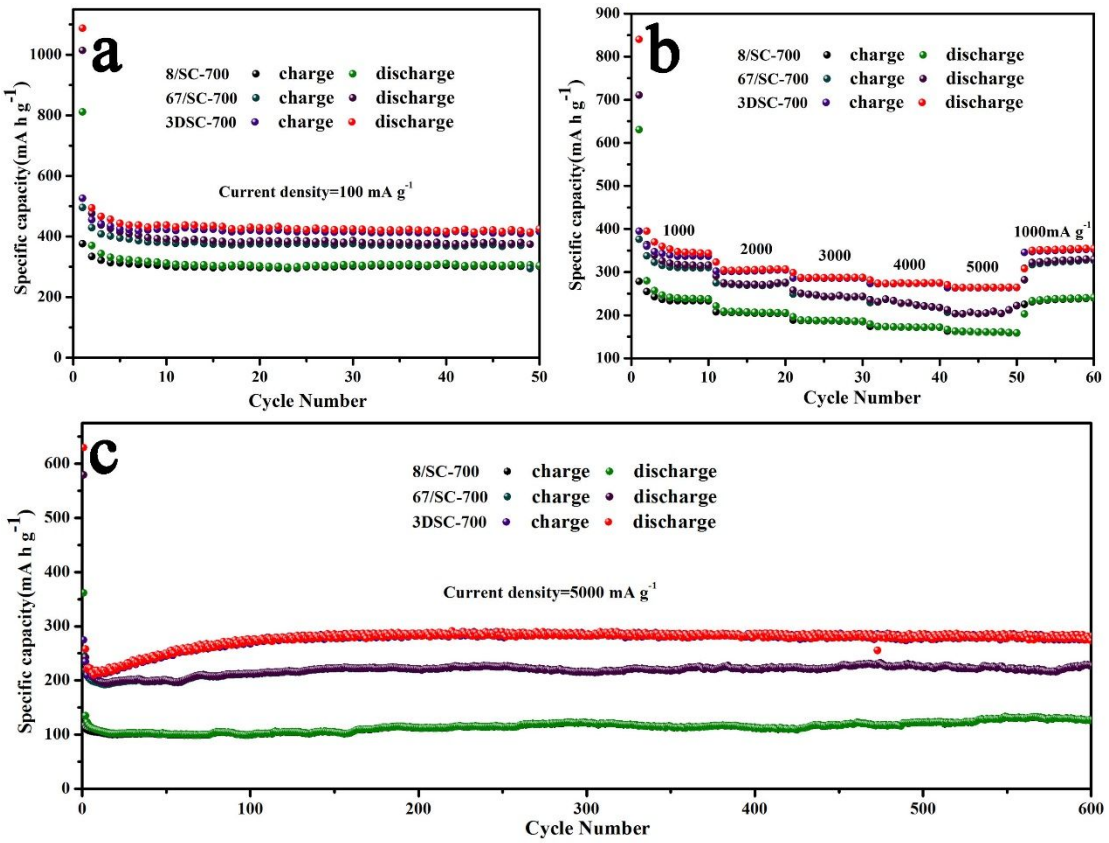

Figure S7. a) Cycling stability of 8/SC-700, 67/SC-700 and 3DSC-700 at a current density of 100 mA/g, b) rate performance of 8/SC-700, 67/SC-700 and 3DSC-700 at various current densities (1000-5000 mA/g), c) cycling stability of 8/SC-700, 67/SC-700 and 3DSC-700 at a current density of 5000 mA/g.

The relationship[7-8] between peak current (i) and scan rate (ν) can be calculated as follow:

$$i=a\nu^{b}=i\,(V)=k_1\nu+k_2\nu^{1/2} \quad (1)$$

In Equation (1), a and b are adjustable values, which can be transformed to

$$\log i= b\log\nu + \log a \quad (2)$$

According to Equation (2), the slope of the log(ν)-log(i) lines are b values. It's worth noting that when the slope is 0.5 (b=0.5), it implies the sodium storage process is diffusion-controlled, and when the slope is 1 (b=1), it reflects the sodium storage is

mainly dominated by surface capacitance.

According to Equation of $i(V)=k_1\nu+k_2\nu^{1/2}$,we can quantify the contribution of surface capacitive-controlled effect ($k_1\nu$) and the diffusion-controlled Na^+ intercalation effect ($k_2\nu^{1/2}$) to the total sodium storage.[7, 9-10] In Equation of $i(V)=k_1\nu+k_2\nu^{1/2}$, i (V) is the detected current response at a fixed potential V, ν is the scan rate, k_1 and k_2 are constants.

Computational methods

First-principles spin-polarized calculations were performed within density functional theory (DFT) implemented in the Vienna *ab initio* simulation package (VASP).[11-12] The projector augmented wave (PAW) method was used to describe the ion-electron electrons interactions.[13] The generalized gradient approximation in the Perdew-Burke-Ernzerhof form[14] was adopted with the cutoff energy set to 450 eV. The convergence criteria for the residual force and energy were set to 0.02 eV/Å and 10^{-5} eV, respectively. The *k*-point meshes with 6×6×1 grid for the 2×2×1 supercell were sampled by the Γ-centered Monkhorst-Pack grids.[15] Bilayer graphene was employed to evaluate the S-doping effect and avacuum slab exceeds 15 Å was employed to avoid the interaction between periodic units. To evaluate the Na diffusion energy barriers, the nudged elastic band (NEB) method was adopted,[16] and four images were inserted between initial and final states. The adsorption energies of Na atoms were calculated by

$$E_b=(E_{n\mathrm{Na@substrate}}-E_{\mathrm{substrate}}-nE_{\mathrm{Na}})/n$$

where $E_{\mathrm{Na@substrate}}$ and $E_{\mathrm{substrate}}$ are the total energies of the substrate with and without Na adsorption, respectively. E_{Na} is the chemical potential of Na leveled from Na metal, and n is the number of adsorbed Na atoms.

Table S1. Elemental analysis of 3DSC-700 and MDC-700

Sample	Chemical composition [wt%]		
	C	N	S
3DSC-700	71.92	0.074	20.10
MDC-700	40.11	8.145	0.155

Table S2. Comparison of the electrochemical performance of various heteroatom doping carbon materials as anodes for SIBs

Samples	S-doping level	Specific capacity (mAh/g)	Current density (mA/g)	Refs.(year)
SC	15.17 wt.%	~ 303.2 （700th）	500	[17]（2015）
		~250	1000	
Sulfur-doped Disordered Carbon	26.9 wt.%	333	100	[6]（2015）
		271（1000th）	1000	
Sulfur covalently bonded graphene	2.29 at.%	262	100	[18]（2015）
		150（200th）	1000	
Sulfur-doped flexible graphene films	16.7 wt. %	244（300th）	100	[19]（2016）
S-Doped N-Rich Carbon Nanosheets	9.19 wt. %	350（100th）	50	[20]（2017）
		211（1000th）	1000	
Sulfur-Doped Graphitic Carbon Nanosheets	2.12 wt.%	321.5（100th）	100	[21]（2017）
		161.8（5000th）	5000	
Sulfur-doped mesoporous carbons	2.5 at. %	188.6（300th）	100	[22]（2017）
		173.7（500th）	200	
S-Doped Hard Carbon	6.3 at. %	320（100th）	100	[23]（2018）
		200（4000th）	1000	
S/N co-doped carbon materials	5.4 wt. %	294（150th）	100	[24]（2018）
N/S-co-doped hollow		329（100th）	100	[25]（2018）

carbon nanofibers		286（2,000th）	1000	
S-doped solvothermal graphene	21.8 wt%	380（300th） 250（1,000th）	100 2000	[26]（2018）
sulfur-doped carbon spheres	25.5 wt%	443.4（50 th） 238.2（600 th）	50 1000	[27] (2017)
This work	20.10 wt. %	~ 450（100th） 225（3000th）	100 5000	

References

1. Chen, Q.; Ren, M.; Xu, H.; Liu, W.; Hei, J.; Su, L.; Wang, L., Cu_2S@ N, S Dual-Doped Carbon Matrix Hybrid as Superior Anode Materials for Lithium/Sodium Ion Batteries. *ChemElectroChem* **2018,** *5*, 2135-2141.
2. Modak, A.; Das, S.; Chanda, D. K.; Samanta, A.; Jana, S., Thiophene Containing Microporous and Mesoporous Nanoplates for Separation of Mercury from Aqueous Solution. *New J. Chem.* **2019,** *43*, 3341-3349.
3. Liu, S.; Zhou, J.; Song, H., 2D Zn-Hexamine Coordination Frameworks and Their Derived N-Rich Porous Carbon Nanosheets for Ultrafast Sodium Storage. *Advanced Energy Materials* **2018**, *8*, 1800569.
4. Li, D.; Zhang, L.; Chen, H.; Ding, L. X.; Wang, S.; Wang, H., Nitrogen-Doped Bamboo-Like Carbon Nanotubes: Promising Anode Materials for Sodium-Ion Batteries. *Chem. Commun.* **2015,** *51* , 16045-16048.
5. Lu, M.; Yu, W.; Shi, J.; Liu, W.; Chen, S.; Wang, X.; Wang, H., Self-Doped Carbon Architectures with Heteroatoms Containing Nitrogen, Oxygen and Sulfur as High-Performance Anodes for Lithium- and Sodium-Ion Batteries. *Electrochim. Acta* **2017,** *251*, 396-406.
6. Li, W.; Zhou, M.; Li, H.; Wang, K.; Cheng, S.; Jiang, K., A High Performance Sulfur-Doped Disordered Carbon Anode for Sodium Ion Batteries. *Energy Environ. Sci.* **2015,** *8*, 2916-2921.
7. Zhu, Y.-E.; Yang, L.; Sheng, J.; Chen, Y.; Gu, H.; Wei, J.; Zhou, Z., Fast Sodium Storage in TiO_2@CNT@C Nanorods for High-Performance Na-Ion Capacitors.

Adv. Energy Mater. **2017,** *7*, 1701222.

8. Chao, D.; Liang, P.; Chen, Z.; Bai, L.; Shen, H.; Liu, X.; Xia, X.; Zhao, Y.; Savilov, S. V.; Lin, J.; Shen, Z. X., Pseudocapacitive Na-Ion Storage Boosts High Rate and Areal Capacity of Self-Branched 2D Layered Metal Chalcogenide Nanoarrays. *ACS Nano* **2016,** *10*, 10211-10219.
9. Chao, D.; Zhu, C.; Yang, P.; Xia, X.; Liu, J.; Wang, J.; Fan, X.; Savilov, S. V.; Lin, J.; Fan, H. J.; Shen, Z. X., Array of Nanosheets Render Ultrafast and High-Capacity Na-Ion Storage by Tunable Pseudocapacitance. *Nat. Commun.* **2016,** *7*, 12122.
10. Augustyn, V.; Simon, P.; Dunn, B., Pseudocapacitive Oxide Materials for High-Rate Electrochemical Energy Storage. *Energy Environ. Sci.* **2014,** *7*, 1597-1614.
11. Kresse, G.; Furthmuller, J., Efficient Iterative Schemes for ab Initio Total-Energy Calculations Using a Plane-Wave Basis Set. *Phys. Rev. B.* **1996,** *54*, 11169-11186.
12. Kresse, G.; Joubert, D., From Ultrasoft Pseudopotentials to the Projector Augmented-Wave Method. *Phys. Rev. B.* **1999,** *59*, 1758-1775.
13. Blochl, P. E., Projector Augmented-Wave Method. *Phys. Rev. B.* **1994,** *50*, 17953-17979.
14. Perdew, J. P.; Burke, K.; Ernzerhof, M., Generalized Gradient Approximation Made Simple. *Phys. Rev. Lett.* **1996,** *77*, 3865-3868.
15. Monkhorst, H. J.; Pack, J. D., Special Points for Brillouin-Zone Integrations. *Phys. Rev. B.* **1976,** *13*, 5188-5192.
16. Henkelman, G.; Jónsson, H., Improved Tangent Estimate in the Nudged Elastic Band Method for Finding Minimum Energy Paths and Saddle Points. J. Chem. Phys. **2000,** *113*, 9978-9985.
17. Qie, L.; Chen, W.; Xiong, X.; Hu, C.; Zou, F.; Hu, P.; Huang, Y., Sulfur-Doped Carbon with Enlarged Interlayer Distance as a High-Performance Anode Material for Sodium-Ion Batteries. *Adv. Sci.* **2015,** *2*, 1500195.
18. Wang, X.; Li, G.; Hassan, F. M.; Li, J.; Fan, X.; Batmaz, R.; Xiao, X.; Chen, Z., Sulfur Covalently Bonded Graphene with Large Capacity and High Rate for High-Performance Sodium-Ion Batteries Anodes. *Nano Energy* **2015,** *15*, 746-754.
19. Deng, X.; Xie, K.; Li, L.; Zhou, W.; Sunarso, J.; Shao, Z., Scalable Synthesis of

Self-Standing Sulfur-Doped Flexible Graphene Films as Recyclable Anode Materials for Low-Cost Sodium-Ion Batteries. *Carbon* **2016,** *107*, 67-73.

20. Yang, J.; Zhou, X.; Wu, D.; Zhao, X.; Zhou, Z., S-Doped N-Rich Carbon Nanosheets with Expanded Interlayer Distance as Anode Materials for Sodium-Ion Batteries. *Adv. Mater.* **2017,** *29*, 1604108.
21. Zou, G.; Wang, C.; Hou, H.; Wang, C.; Qiu, X.; Ji, X., Controllable Interlayer Spacing of Sulfur-Doped Graphitic Carbon Nanosheets for Fast Sodium-Ion Batteries. *Small* **2017,** *13*, 1700762.
22. Shi, X. D.; Chen, Y. X.; Lai, Y. Q.; Zhang, K.; Li, J.; Zhang, Z. A., Metal Organic Frameworks Templated Sulfur-Doped Mesoporous Carbons as Anode Materials for Advanced Sodium Ion Batteries. *Carbon* **2017,** *123*, 250-258.
23. Hong, Z.; Zhen, Y.; Ruan, Y.; Kang, M.; Zhou, K.; Zhang, J. M.; Huang, Z.; Wei, M., Rational Design and General Synthesis of S-Doped Hard Carbon with Tunable Doping Sites toward Excellent Na-Ion Storage Performance. *Adv. Mater.* **2018**, *30*, 1802035.
24. Zhao, G.; Zhang, Y.; Zou, G.; Zhang, Y.; Hong, W.; Jiang, Y.; Xu, W.; Shuai, H.; Hou, H.; Ji, X., Evaluating the Influences of the Sulfur Content in Precursors on the Structure and Sodium Storage Performances of Carbon Materials. *J. Mater. Chem. A.* **2018,** *6* , 11488-11495.
25. Luo, Z.; Liu, S.; Cai, Y.; Li, S.; Pan, A.; Liang, S., Nitrogen/Sulfur Co-Doped Hollow Carbon Nanofiber Anode Obtained from Polypyrrole with Enhanced Electrochemical Performance for Na-Ion Batteries. *Sci. Bull.* **2018,** *63*, 126-132.
26. Quan, B.; Jin, A.; Yu, S. H.; Kang, S. M.; Jeong, J.; Abruna, H. D.; Jin, L.; Piao, Y.; Sung, Y. E., Solvothermal-Derived S-Doped Graphene as an Anode Material for Sodium-Ion Batteries. *Adv. Sci.* **2018,** *5*, 1700880.
27. Tang, H.; Yan, D.; Lu, T.; Pan, L., Sulfur-Doped Carbon Spheres with Hierarchical Micro/Mesopores as Anode Materials for Sodium-Ion Batteries. *Electrochim. Acta* **2017,** *241*, 63-72.